Carbohydrate Polymers 83 (2011) 246–256

Contents lists available at ScienceDirect

Carbohydrate Polymers

journal homepage: www.elsevier.com/locate/carbpol

Three-phase model and digital image correlation to assess the interphase effect on the elasticity of carbohdyrate polymer-based composites reinforced with glass–silica beads

S. Rjafiallah, S. Guessasma *

INRA, UR1268 Unité Biopolymères Interactions et Assemblage (BIA), Rue de la Géraudière, F-44000 Nantes, France

ARTICLE INFO

Article history:
Received 7 May 2010
Received in revised form 2 July 2010
Accepted 27 July 2010
Available online 6 August 2010

Keywords:
Biopolymer–matrix composites
Interphase
Finite element analysis
Digital image correlation
Microstructure

ABSTRACT

Thermomoulding of starch-based composite shows that the elastic modulus is non-linearly dependent on the fraction of glass–silica used as a reinforcement material. In order to explain this result, a three-phase model is implemented using finite element computation to account for the role of phase arrangement and interphase properties on the effective behaviour. For this purpose, virtual generation of typical microstructures is performed taking into account the size distribution of the filler as well as the interphase properties. The numerical results well show that, depending on the interphase modulus, two opposite trends are predictable. The identification of the experimental elastic behaviour points out the weak interface adhesion between the matrix and the filler. This result is confirmed by the digital image correlation, which depicts a displacement jump across the starch–glass–silica interface.

1. Review of recent contributions

Several decades ago, biopolymers were mainly used in food applications. Nowadays, biodegradability has become a targeted property thanks to the environmental restrictions and policies (Gross & Kalra, 2002). The use of biomaterials in non-food applications has become more than a pure scientific thought (Giancaspro, Papakonstantinou, & Balaguru, 2008; Ma & Wen, 2008; Tharanathan, 2003). In regard to these matters, intensive work has been dedicated to the study of biomaterial properties (Beg, Pickering, & Weal, 2005; Gáspár, Benkő, Dogossy, Réczey, & Czigány, 2005; Kim, 2008; Kunanopparat, Menut, Morel, & Guilbert, 2008; Wu, Sakabe, & Isobe, 2003). In our study, the targeted materials are starch-based composites reinforced by glass–silica particles. The purpose of this study is to implement a mechanical model that is able to quantify both the effect of phase arrangement and mechanical contrast between intrinsic phases on the effective elasticity behaviour.

We give a particular attention to the imperfect interphase layer between the biopolymer–matrix and the inorganic reinforcement. Such an attention is justified by the primarily role of the interphase properties as recognised for varieties of materials and in the present case. It is also justified by the water mobility in biopolymer materials (Li, Dickinson, & Chinachoti, 1998), which causes evolving spatial distribution of water content (Ruan et al., 1996), especially for composites where phases have different equilibrium water contents (Rjafiallah, Guessasma, & Lourdin, 2009). The study of the interphase role has thus been described numerically, experimentally and analytically in the case of composites reinforced by fibres (Agbossou, 1995; Chaboche, Girard, & Schaff, 1997; Cheeseman & Santare, 2001; Naslain et al., 1999; Scheffler et al., 2009; Shen & Li, 2005; Taliercio, 2007), particulate composites including nano-scale structures (Duan, Wang, Huang, & Karihaloo, 2005; Hashin & Monteiro, 2002; Lutz & Zimmerman, 2005; Papanicolaou, Xepapadaki, Kotrotsos, & Mouzakis, 2008; Sevostianov & Kachanov, 2007; Shen & Li, 2005; Wang & Meguid, 1999; Wang & Zhong, 2003; Wei & Huang, 2004), multi-layered systems (Alem & Dravid, 2008; Alfano & Criseld, 2001; Chu & Rokhlin, 1995; Pompidou & Lamon, 2007; Ru, 1999), textured materials (Weissmuller & Cahn, 1997) and more recently in randomly structured composites (Rjafiallah, Guessasma, & Lourdin, 2009). We recall the definition of a perfect interface as the interface allowing continuity of both traction and displacement across the interface (Hashin, 2002). If one of these conditions is not fulfilled, imperfect interface is rather used to qualify such an interface. The interface between two solids has a zero-thickness or a sharp profile whereas the interphase has a finite-thickness. The distinction becomes more subtle if we refer to different studies using interface representation of the interphase as described later or when nano-sized fillers are used (Sevostianov & Kachanov, 2007a). In some cases, it is suitable

* Corresponding author. Tel.: +33 0 240675036; fax: +33 0 240675036.
E-mail address: Sofiane.guessasma@nantes.inra.fr (S. Guessasma).

0144-8617/$ – see front matter © 2010 Elsevier Ltd. All rights reserved.
doi:10.1016/j.carbpol.2010.07.055

to average the interface effect using the interphase representation, especially if we do not have access to the physics of interface bonding. Nanoindentation provides, for example, such information since the indent combines both the intrinsic material and interface responses (Guessasma, Sehaki, Lourdin, & Bourmaud, 2008). Physical interphases are needed because they provide chemical compatibility to promote mechanical as well as thermal properties (Chaudhry, Ho, Drzal, Harris, & Laine, 1995; Igawa, Taguchi, Yamada, Ishii, & Jitsukawa, 2007; Lipkin, Clarke, & Evans, 1998). Interphase can also be an inherent feature of the forming process like in concrete (Garboczi & Bentz, 1997; Sun, Garboczi, & Shah, 2007). As a result of processing, varied properties across the interface are either observed or anticipated (Naslain et al., 1999). In some fibrous composites, the presence of fibre flaws influences the stress distribution a short distance away from the fibre–matrix interface (Ru, 1999; Scheffler et al., 2009). In the present case, the interphase refers to this particular case where the interfacial region is affected by local variability of the water content in the matrix and thus changing in turn the mechanical properties in this region. Such feature was previously suggested to explain the mechanical behaviour of a fully biopolymer composites (Rjafiallah, Guessasma, & Lourdin, 2009). The effect of water content on the mechanical behaviour of starch-based materials is well known. For example, Biliaderis, Lazaridou, and Arvanitoyannis (1999) have shown that Young's modulus of starch-based blends decreases when the water content in the material increases. The measurement of the interphase properties is accessible experimentally using classical methods such as pull out, push-out tests (Chandra & Ananth, 1995; Chandra & Ghonem, 2001; Nozawa, Katoh, & Snead, 2009) and fragmentation test (Johnson, Hayes, & Jones, 2009; Tripathi & Jones, 1997; Zhou, Wagner, & Nutt, 2001), particularly for fibre-reinforced materials. Local measurement based on indentation are also utilised preferentially for thin films (Chicot, Démarécaux, & Lesage, 1996; Dehm, Ruhle, Conway, & Raj, 1997; Ho & Dual, 1996; Kharrat, Chateauminois, Carpentier, & Kapsa, 1997; Lee, Wang, Pharr, & Xu, 2007; Li & Siegmund, 2004; Zhang, Chen, & Li, 2004; Zhu & Bartos, 1997). Microscopy-based techniques like the scanning force microscopy are also known (Liu et al., 2008; Munz, Sturm, Schulz, & Hinrichsen, 1998; Tillman, Hayes, & Seferis, 2000). Indirect and non-destructive techniques like with ultrasound were developed by Rokhlin and co-workers (Rokhlin & Huang, 1998; Rokhlin, Huang, & Chu, 1995). In the present study, strain field measurement near the interface is performed using 2D image correlation to give evidence of imperfect interphase properties. This approach is relatively new with regard to its potential application to describe interface properties (Mann, Miller, Race, & Verdonschot, 2009). In complement, we have developed a finite element model to account for the imperfect interphase between the starch matrix and glass–silica particles. This model accounts also for the spatial distribution of the phases and thus explicitly integrates all these features in the microstructure. This approach is thus a numerical extension of the three-phase model at the microstructure scale. Three-phase model is classically used to handle the effect of a third phase on the overall behaviour of composites. First developments of this idea are based on an analytical description of the intimate filler–matrix environment. In several 2D studies, the conceptual model consists of centred filler surrounded by a finite-thickness third phase and imbedded in a finite or infinite matrix (Lutz, Menteiro, & Zimmerman, 1997; Lutz & Zimmerman, 1996; Tasdemir et al., 1998). The problem is solved using different formulations (Garboczi & Bentz, 1997; Shen, Schiavone, & Potapenko, 2005) and homogenisation rules are applied to derive the effective laws. Attempts were made to improve the analytical description of the phase arrangement using for example the interface representation of the interphase layer (Benveniste, 2006). Such approach is mainly justified by the fact that the bonding between phases is not necessarily dependent on the physical interphase rather on the contact physics. Within this approach, both isotropic and anisotropic behaviours of the interphase layer were addressed (Benveniste, 2006; Hashin, 2002). Effective medium theory was also introduced to study the effective properties in presence of interfacial zone (Garboczi & Berryman, 2001). The main body of the method resides in the replacement of the three-phase problem by a two-topological phase model and making use of differentiation principles to derive expressions for the effective properties. Numerical simulation based on continuum mechanics was also considered (Chandra & Ananth, 1995) particularly combining unit cell model and finite element technique (Esmaeili & Tomita, 2006; Taliercio, 2007; Zhang, Li, & Wang, 2007). The interphase layer is assumed to be either constituted of volumic elements (Ash, Cross, Svalstad, Kellar, & Kjerengtroen, 2003; Chaboche et al., 1997; Lee et al., 2007; Tsui, Tang, & Lee, 2001) as the approach shown here or by using interface elements obeying to different interface laws among them spring-like and cohesive zone models (Alfano & Criseld, 2001; Chaboche et al., 1997; Guessasma & Benseddiq, 2009; Lissenden & Herakovich, 1995; Segurado & LLorca, 2004).

The link between both interface and interphase models has been recognised as dependent on the traction–displacement relationship (Wang, Duan, Zhang, & Huang, 2005). When assuming proportionality between the traction and displacement across the interface (i.e., the use of spring constant terms), this is equivalent to more or less compliant thin interphase conditions (Benveniste & Miloh, 2001; Hashin, 2002). Non-linear proportionality between traction and displacement is exploited in the progressive decohesion of the interphase and crack extension (Chaboche et al., 1997; Segurado & LLorca, 2004; Tvergaard, 2009). The way the interphase influences the effective properties depends on the contrast between the properties of the interphase and the remaining phases (Esmaeili & Tomita, 2006; Liu et al., 2008; Taliercio, 2007; Wei & Huang, 2004), on the interphase thickness-filler size ratio (Kari et al., 2008; Sevostianov & Kachanov, 2007) and finally the ability to form a connected interphase network (Rjafiallah, Guessasma, & Lourdin, 2009). In such a way, a strong interphase effect is expected, for example, for those composites reinforced by nano-sized particles, as a consequence of the large volume content of interfaces (Patel, Bhattacharya, & Basu, 2008). The present finite element model has the advantage to handle all these features numerically since the above-mentioned models fail in describing a varied "environment" around the fillers especially when particle interspacing becomes small. Some recent contributions tend towards such description using finite element modelling (Kari et al., 2008). The interphase structure has been accounted either by considering uniform properties (Hashin & Monteiro, 2002) or varied properties (Li, 2000; Lutz et al., 1997; Lutz & Zimmerman, 2005; Ru, 1999; Wang & Zhong, 2003).

Exact solutions of the effective bulk modulus have been obtained in the case of a varied interphase properties (Lutz & Zimmerman, 2005). Inverse techniques were also used to determine uniform interphase properties like with the generalised self-consistent scheme (Hashin & Monteiro, 2002). In our model, we assume that the interphase properties are constant across the interfacial zone, which constitutes our main hypothesis. Despite that this hypothesis is restrictive, it constitutes the simplest case for which the interphase problem can be handled using a unique descriptor, i.e., interphase thickness. A graded material would reflect better the physics of the interphase formation since the transition from the filler to the matrix properties can be correctly described using a specific profile (Lutz et al., 1997; Lutz & Zimmerman, 2005). Indeed, local testing techniques have been utilised for the assessment for the exact profile of such as indentation, scratch and AFM experiments (Choi et al., 2008; Gao & Mader, 2002). Exponential profiles have been identified at a relatively small scale testing (Munz et al.,

1998). For an intermediate scale testing of few microns, more linear transitions are observed (Urena, Rams, Escalera, & Sanchez, 2005). For glass–polymer systems, linear increase of the hardness have been experimentally determined for interphase widths of about 100 μm (Hodzic, Stachurski, & Kim, 2000).

Numerical handling of varied mechanical properties across the interphase requires several descriptors and constitutes a refinement that adds much complexity to the present problem.

We should mention, finally, that the above-mentioned research works are given as a support to situate our present model with regard to the exhaustive literature published in the subject. Within the context of interphase effect in the mechanics of composites, the reader may find some missing references or relevant works that are not named here, especially those which appeared before the middle of the 90s.

2. Experimental layout

Composite fabrication includes a preprocessing step of the starch matrix in order to obtain granules of an amorphous material. The detailed description of this step is given in (Rjafiallah, Guessasma, Chaunier, & Lourdin, 2009). Such a preprocessing step requires extrusion of native (semi-crystalline) starch followed by cryogrinding and finally storage for at least 15 days before performing further steps. Moisture content of the powder is adjusted in a confined NaBr environment at a relative humidity of 59% and at room temperature. The final moisture content of amorphous starch is 16% after three days of storage. The reinforcement material is the glass–silica purchased from SOVITEC[1]. The analysis of the glass–silica powder morphology is determined using SEM analysis. Particle morphology is spherical with size in the range (20–50 μm) and an average size of about 35 μm. Starch powder is mixed to different glass–silica contents ranging from 1.25 to 30 wt.%. The powder is thermomoulded for 10 min at 140 °C under a pressure of about 42 MPa. Thermomoulded strips of dimensions 35 mm × 10 mm × 1.2 mm are again stored in a confined environment, where the final moisture content is 12%. Under these conditions, the designed composites are in the glassy state. Fig. 1 shows cross section views of the designed material for two different filler fractions.

Since the material is brittle, micro-cracks are apparent in the microstructure as a consequence of cross-sectioning. The adhesion between glass–silica particles and the starch matrix remains stable even at large filler fractions. No complete debonding is observed after the forming process. SEM analysis indicates thus that wetability of the matrix is acceptable in the considered filler fraction range (Fig. 2).

For the experiments dealing with image correlation, macroscopic glass beads of size 2 mm are used. The idea is to allow a surface observation of the glass–starch interface by carefully positioning the glass bead during the thermomoulding process. Such positioning is obtained by modified the mould in order to allow half of the bead to remain out of the top surface of the sample (Fig. 3a).

In such a way, the interface is visible along the largest circumference while testing. The choice of using a macroscopic bead instead of a microscopic one is of course due to the limited resolution of the digital camera. This particular choice should not alter the conclusions of the image correlation, since the measured displacements are computed with a subpixel accuracy. Uniaxial loading is undertaken using a micromechanical test equipment. Traction is performed under a constant displacement rate of 10 μm s^{-1} up to a maximum displacement of 3 mm. Young's modulus is derived from the linear part of the stress–strain curve. Five samples per condition are used to study the elastic response.

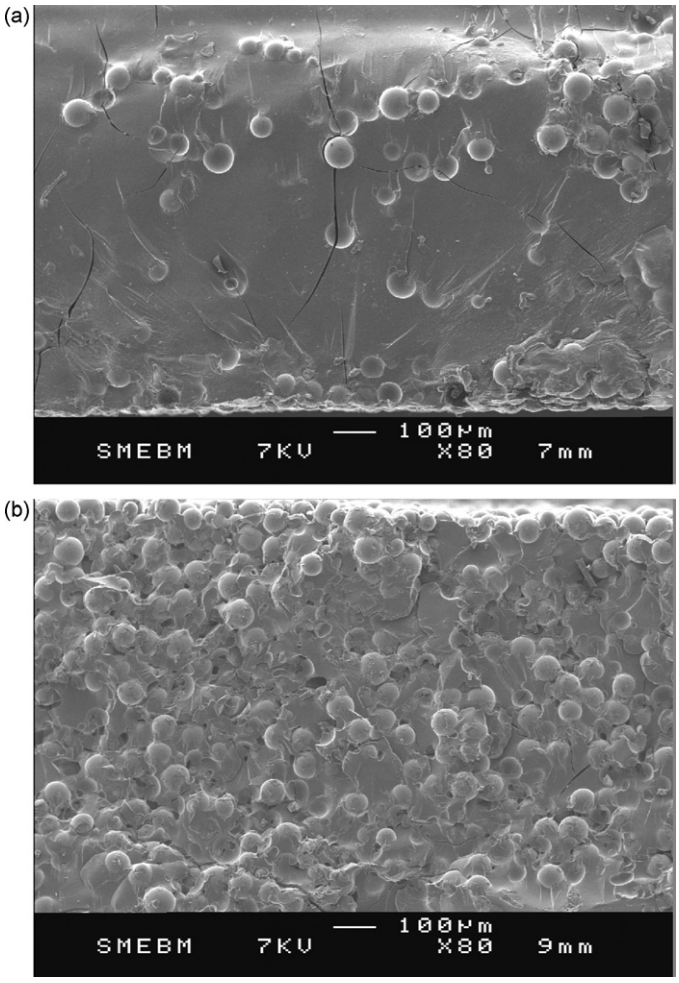

Fig. 1. Typical microstructures of starch-based composite containing: (a) 10% and (b) 30% of glass–silica.

As introduced earlier, testing of strips containing a centred macroscopic glass bead is coupled to a digital camera and a stere-

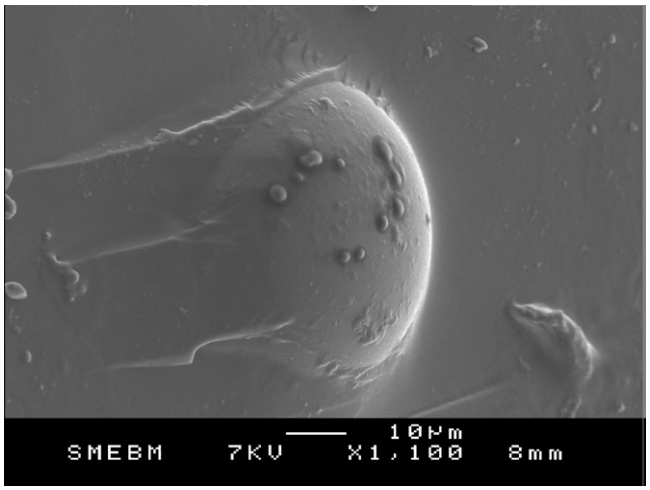

Fig. 2. Magnified view showing the starch–glass–silica interface.

[1] SOVITEC, 163–167 Avenue Georges Pompidou, 33500 Libourne, France.

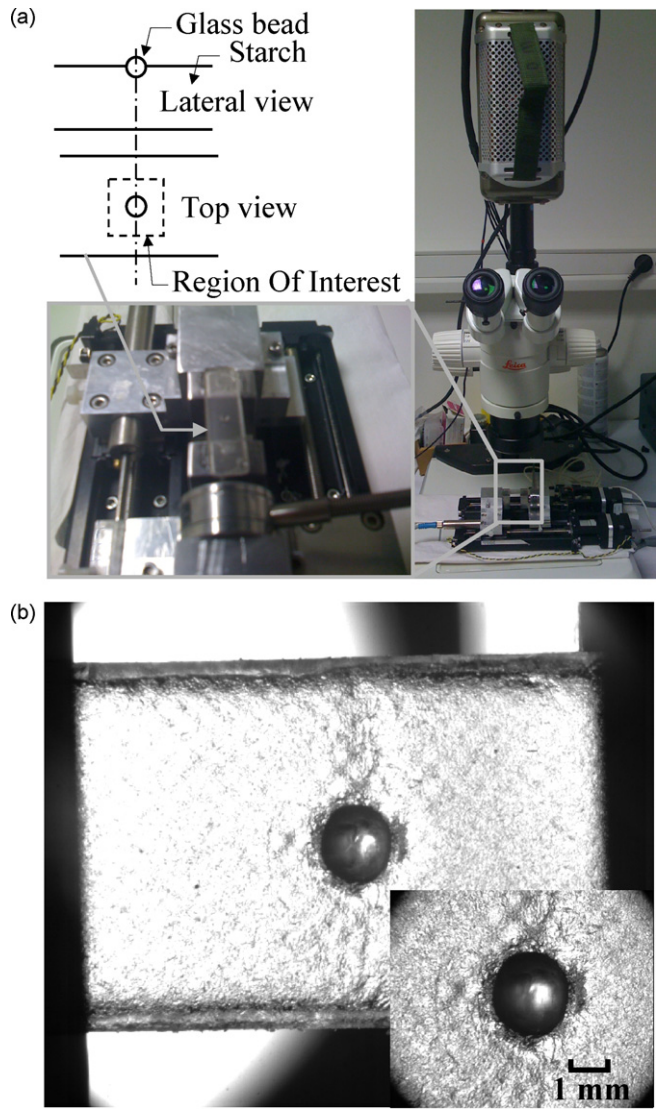

Fig. 3. (a) Micromechanical testing to evaluate interphase properties. (b) Sample bright field observation using transmitted light under a stereomicroscope.

omicroscope to allow displacement field to be acquired while material testing. The image acquisition rate is fixed to 10 frames s^{-1} with an adapted exposure time. In order to assess the displacement field near the glass–matrix interface, the region of interest is centred around the glass bead with a resolution of 600×350 pixels (Fig. 3b). Adequate combination of magnification and resolution is used to deliver precise measure of the displacement field. The complete experimental set-up is illustrated in Fig. 3. Due to transparency of the samples, a surface texture is created to allow image correlation to be applied. During the forming process, a Teflon cover is used between the sealing bloc and the pressed powder. The traction is performed with a constant displacement rate of 40 $\mu m\, s^{-1}$ up to a loading force of 120 N. Under these testing conditions, the behaviour of the material remains elastic. The displacement field measurement is performed using the freely available image correlation toolbox developed under MATLAB environment by the group of Kevin J. Hemker at the Johns Hopkins University. Basically, the image correlation stands on the ability to correlate the grey levels of a given ROI (region of interest) at a given time to another ROI after a time increment. The problem is thus a non-linear optimisation process, which aims at predicting the displacement of the centre of the ROI based on the grey level correlation. A typical objective function describing the minimisation principle is for example:

$$g = 1 - \frac{(\gamma(x_i, y_j) - \gamma_m)(\gamma'(x'_i, y') - \gamma'_m)}{\sqrt{(\gamma(x_i, y_j) - \gamma_m)^2 (\gamma'(x'_i, y') - \gamma'_m)^2}} \quad (1)$$

where γ is the grey level at a particular position (x_i, y_i) within a given subimage. γ' has an equivalent definition but for the deformed submiage (Fig. 3). γ_m and γ'_m are the average grey levels within the undeformed and deformed subimages, respectively. Note that Einstein notation is used, for which the indices i and j run over all the pixels in the considered subimages. The coordinates (x_i, y_j) and (x'_i, y'_j) belong to particular positions in the undeofrmed and deformed subimages.

The image correlation supposes that the couples (x_i, y_j) and (x'_i, y'_j) are related by means of their corresponding grey levels in the sense that all grey levels in the deformed subimages are uniquely correlated to those in the deformed subimage. It comes immediately that,

$$x'_i = x_i + u + \frac{\partial u}{\partial x}\Delta x + \frac{\partial u}{\partial y}\Delta y \quad (2)$$

and

$$y'_i = y_i + v + \frac{\partial v}{\partial x}\Delta x + \frac{\partial v}{\partial y}\Delta y \quad (3)$$

where (u, v) is the displacement vector of the ROI centre towards the deformed position.

The lowest score of g corresponds to the most probable shift of the ROI within a time increment whereas the size of the submiage corresponds to the resolution of the correlation grid. In our case, subimages are square domains of area 10×10 pixels.

3. Modelling technique

In a 2D grid (512×512 pixels), generation of virtual microstructures with similar features to real composites is performed. Random arrangement of discs is controlled using a Gaussian distribution of particle radii. In particular, both the centre (R) and the width (W) of the distribution are varied. The total number of particles is tuned to obtain a given fraction (f). Particles are not allowed to overlap, which fixes an upper limit of the fraction that can be reached. This limiting fraction depends on the generation parameters (W, R) and does not exceed 30%. The generated microstructures are converted into a finite element mesh using square elements. To each pixel in the image corresponds a 4-node element, where each node is capable of translations in X- and Y-directions. The starch matrix is an isotropic material with the following properties: $E_S = 2.62$ GPa, $\nu_S = 0.35$, where E, ν and s hold for Young's modulus, Poisson ratio and starch, respectively. In a similar way, isotropic glass–silica properties are associated to the circular particles ($E_G = 70$ GPa, $\nu_G = 0.18$). In addition to the intrinsic phases, an interphase layer is implemented where a switch from the matrix to the reinforcement is detected. Despite that varied properties across the interface are expected as in the case of several polymer–glass systems (Hodzic et al., 2000), we simplify the problem by assuming that such variations are equivalent to the action of an interphase having a constant thickness. We know also that interphase thickness may vary depending on the measured property. In the case of hardness score, the interphase thickness is determined by the region affected by plastic deformation. We deal, in our study, with a unique interphase thickness because we are interested in the modulus of elasticity.

The interphase has isotropic properties (E_I varied, $\nu_I = 0.35$) and a finite-thickness (t). In order to account for all possible interphase effects, E_I is varied in a wide range: $E_I = (0.05, 0.1, 10, 30, 80, 90$ GPa). In addition, the interphase layer is varied from 1 to 4 pixels, where

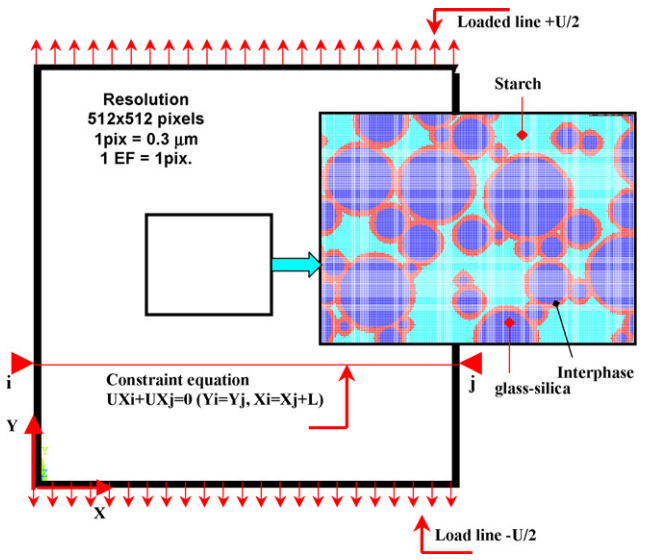

Fig. 4. Typical loading conditions performed on a generated microstructure with interphase effect.

1 pixel = 0.3 μm. Interphase thickness is normalised with respect to the average size of the glass particles. In order to compute the effective Young's modulus, the following loading conditions are used (Fig. 4).

All nodes belonging to the lower and upper lines are displaced by opposite amounts in *Y*-direction to simulate traction. These nodes are free to move in *X*-direction.

Transverse degrees of freedom (UX) of homologue nodes are coupled.

Young's modulus is computed based on the reaction forces and knowing the imposed deformation at the loaded lines. Finite element computation is conducted under plane stress and linear elastic conditions. At least four levels are used for each parameter (W, R, f, E_I, t) of the model. The total number of combinations is 1535.

4. Results and discussion

4.1. Experimental evidence of varied mechanical properties across the interface

Fig. 5 shows the temporal evolution of the displacement field in *X*-direction for a sample containing one glass bead.

The displacement jump across the interface is clearly depicted. Its magnitude increases regularly as function of loading. The analysis of the displacement profile across the glass bead reveals that, for an imposed strain value $\varepsilon = 0.2\%$ (Fig. 5b), the interphase thickness is about 215 μm, irrespective of the profile orientation. The average displacement magnitude is 10 μm. When increasing further more the load (Fig. 5d), the displacement jumps across the interphase are noisier. The average thickness is 269 μm, whereas the average magnitude of the displacement is 27 μm. Strain field corresponding to different storage durations are shown in Fig. 6.

Large storage duration is thought to allow a better local equilibrium of water content. We expect that the corresponding samples will have more homogeneous properties. Fig. 6 depicts that change in storage durations from 3 up to 8 days affects the interphase thickness (between 140 and 169 μm). However, the strain field remains inhomogeneous even for the largest storage duration. Such a result indicates that starch–glass–silica interphase represents a ratio of 7–8% of the glass bead size.

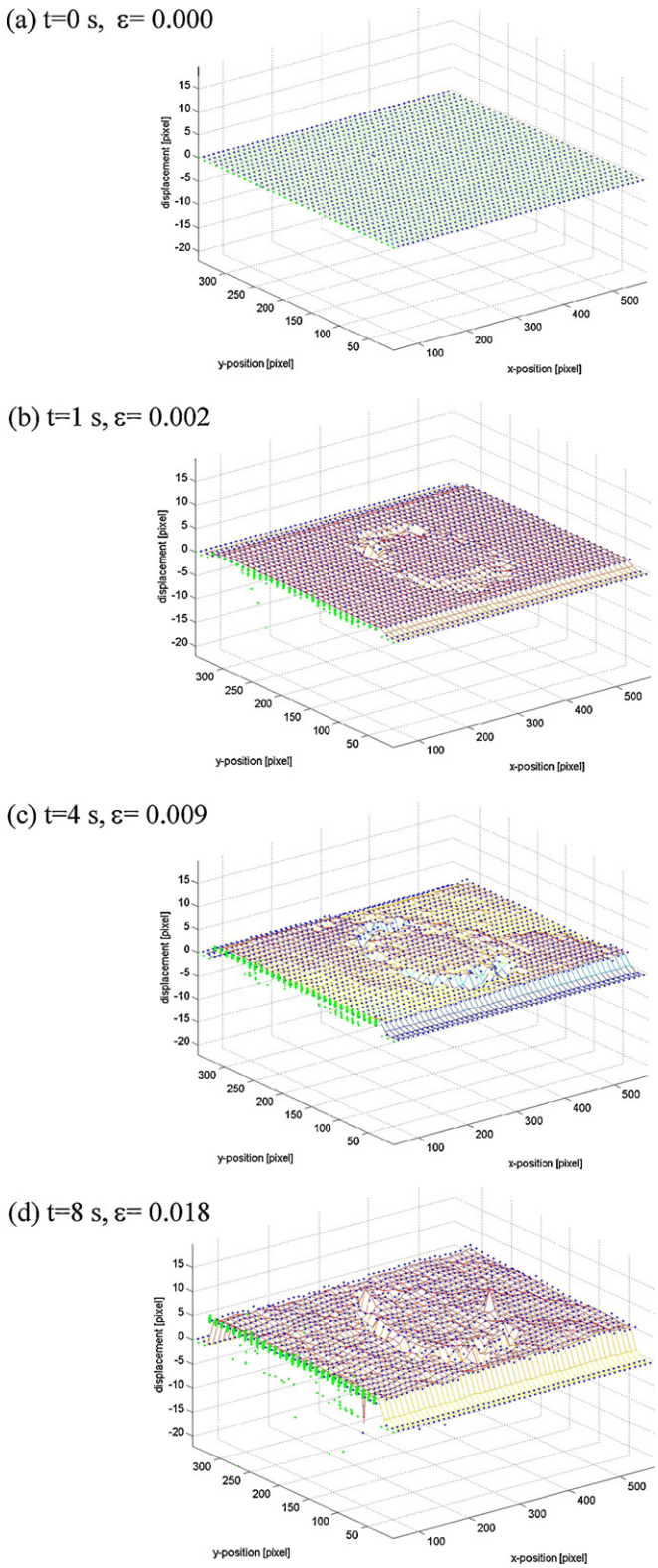

Fig. 5. Time (t) evolution of the displacement pattern. ROI size = 608 × 352 pixels, pixel size = 8.1 μm, sample displacement rate 20 μm/s. The engineering strain (ε) corresponding to each map is also indicated.

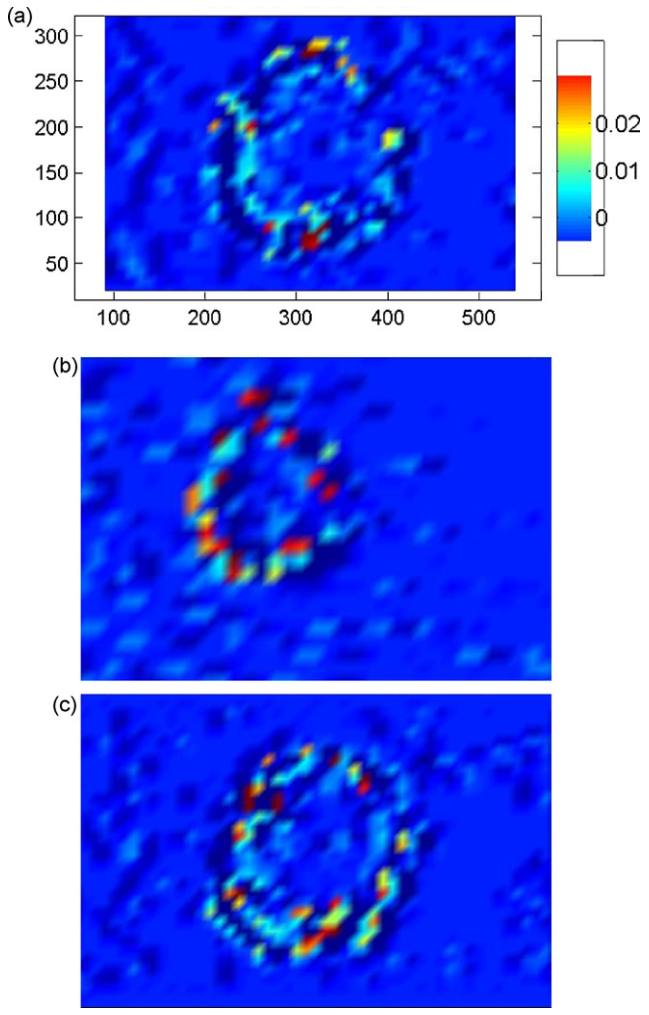

Fig. 6. Strain pattern across the interface as function of storage time. The same scaling is used for each case.

4.2. Sensitivity analysis

The interphase effect can be decoupled into two main contributions. One is related to the nature of the interphase itself. E_I is the parameter that influences the quality of the interphase. The other influential parameter is related to the interphase quantity (q). The last parameter is controlled using R, W, f and t. Fig. 7 depicts the effect of all studied parameters on the interphase content. The increase of q is correlated to the decrease of the centre of radii distribution (R).

Indeed, when the whole distribution is shifted toward small radii, the ratio particle perimeter over area decreases when the particle radius increases. In a similar way, the number of small particles is larger when the size dispersion is increased (Fig. 7b). The total interphase area is positively correlated to the increase of interphase thickness (Fig. 7c). Note that all studied parameters have a linear effect on the interphase quantity but their combinations lead to a highly non-linear effect. Indeed, considering all possible combinations, the interphase quantity (q) is related to R, W, f and t using au automatic fitting routine. The result of the fitting suggests a complex relationship of the form:

$$q(f,W,R,th) = b_{00}th^{b_{01}}R^{b_{02}} + b_{10}th^{b_{11}}R^{b_{12}}W + f\left(a_{00}th^{a_{01}}R^{a_{02}} + a_{10}th^{a_{11}}R^{a_{12}} \exp\left(\left\{a_{20} + \frac{a_{21}}{th} + \frac{a_{22}}{R} + \frac{a_{23}}{th^2} + \frac{a_{24}}{R^2} + \frac{a_{25}}{thR}\right\}W\right)\right) \quad (4)$$

where all fitting parameters are summarised in Table 1.

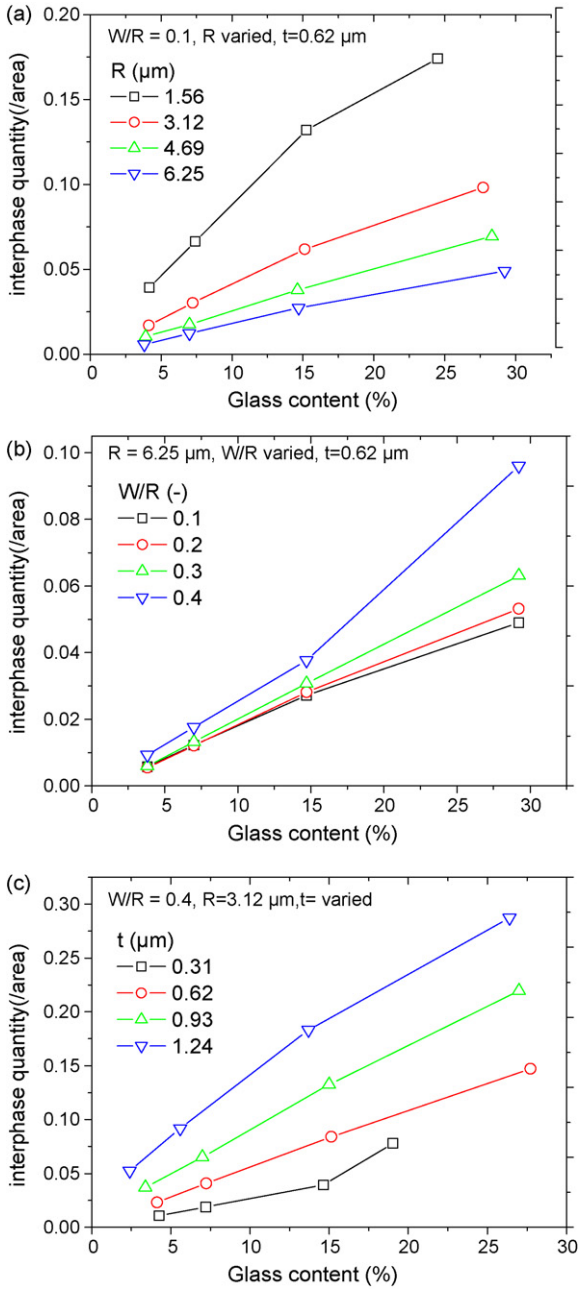

Fig. 7. Effect of the generation parameters on the interphase quantity. (a) Centre of particle radii distribution. (b) Width of radii distribution.

Fig. 8 shows the fitting result using the above equation for all conditions. In this case, the correlation factor is quite satisfying ($R^2 = 0.98$).

The interphase quantity is related to the effective Young's modulus (E_F) depending on the choice of the interphase modulus. Fig. 9 shows the predicted correlations.

When the interphase modulus is lower than that of the matrix, the effective property decreases with the increase of interphase quantity (Fig. 9a). In the opposite case (i.e., $E_I > E_S$), a large interphase modulus is responsible for the increase of the effective modulus but in a more scattered way. This scatter is attributed to size-mixture effect that allows a variability of phase arrangement. The predicted trends shown earlier are in qualitative agreement with the work of Kari et al. (2008) who considered the interphase effect in a virtual composite reinforced by rigid spherical fillers. In their work, the authors showed that depending on the interphase

Table 1
Fitting parameters of the function describing the interphase quantity as function of generation parameters.

	i	j					
		0	1	2	3	4	5
a	0	0.02	1.43	−0.69	–	–	–
	1	−0.01	1.57	−0.60	–	–	–
	2	−1.35	2.18	11.0	−1.77	−15	−15
b	0	0.00	0.40	5.0	0.40	–	–
	1	2.17	−1.97	–	–	–	–

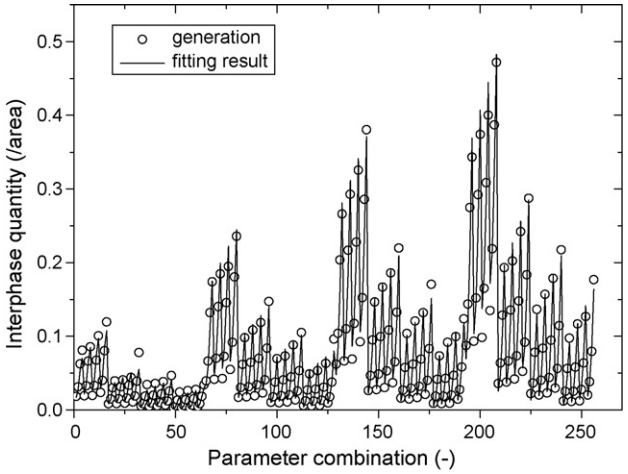

Fig. 8. Fitting results with a non-linear function applied to all possible parameter combinations.

modulus, the effective property is either decreasing or increasing. Note that the exponential decrease of the effective Young's modulus identified in their work is similar to that observed here. Since the apparent correlations in Fig. 9 are simple non-linear functions compared to the case of interphase quantity, it is better to correlate E_F to q. The following relationship is derived from the fitting of the curves shown in Fig. 9.

$$E_F(q, E_I) = E_0 + q_0 \exp\left(-\frac{q}{q_1}\right) \quad (5)$$

where E_0, q_0 and q_1 are all linear functions with respect to E_I.

The fitting parameters are given in Table 2 for both conditions: $E_I > E_S$ and $E_I < E_S$.

4.3. Prediction of the starch–glass–silica interphase properties

Experimental testing of the studied materials reveals a brittle behaviour. The studied composites exhibits a linear increase of the stress up to the ultimate failure, similarly to typical brittle–matrix composites (Lamon, 2001). Fig. 10 depicts the effect of glass–silica content on the measured modulus. The highest modulus is observed for a glass fraction of 2.5%.

Table 2
Fitting parameters describing the non-linear function between the effective modulus and interphase quantity.

	i	j	
		Constant	Slope with respect to E_I/E_S
$E_I < E_S$	E_0	0.05	0.65
	q_0	0.86	4.00
	q_1	0.09	2.52
$E_I > E_S$	E_0	−9.15	0.26
	q_0	10.2	−0.26
	q_1	−1.68	0.04

Beyond this fraction, the composite modulus tends towards its asymptotic value $1.4E_S$. The comparison between the present results and the model of Hashin-Shtrikman shows clearly that the rigidity of the composite is lowered by the presence of a weak interphase region between starch and glass–silica particles. Note that the complete debonding is not a realistic hypothesis in our case because, first, the elastic modulus remains stable beyond 5% of reinforcement content and, second, no material loss is observed after processing especially for those samples with a large glass bead fractions (Fig. 1b). In order to identify the interphase properties associated to the studied composite, an inverse strategy is undertaken. Giving the experimental radius distribution of the glass–silica particles, different combinations of E_I and t are tested in order to fit the experimental behaviour. Image analysis of the size distribution performed on glass–silica reveals the following parameters: $R = 18\ \mu m$ and $W = 8\ \mu m$. Giving an experimental glass fraction, say for example $f = 1.25\%$, it is possible to predict the corresponding interphase quantity using Eq. (4). The result is replaced in

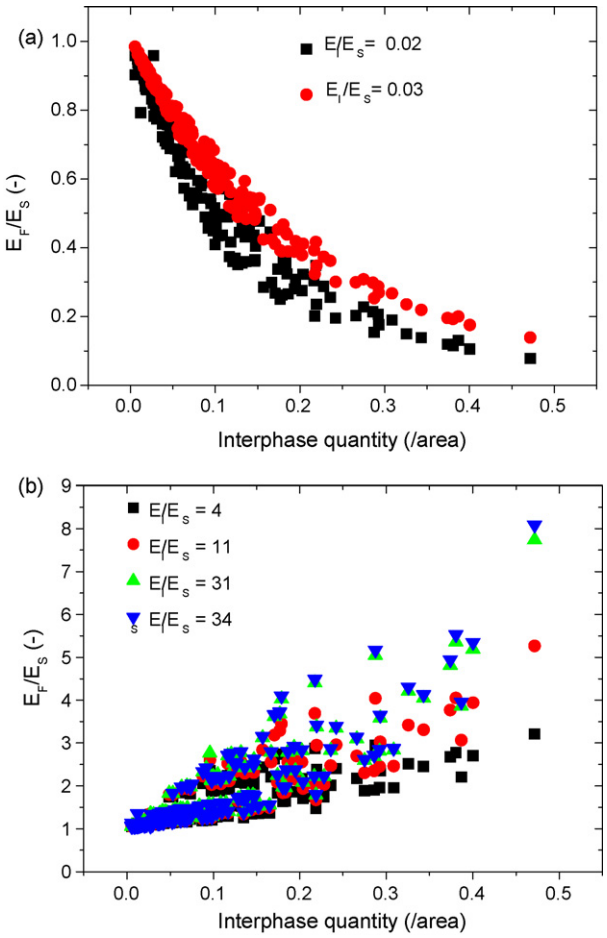

Fig. 9. (a) and (b) Predicted effective modulus tendencies as function of interphase quantity and interphase modulus. Each point represents a FE run.

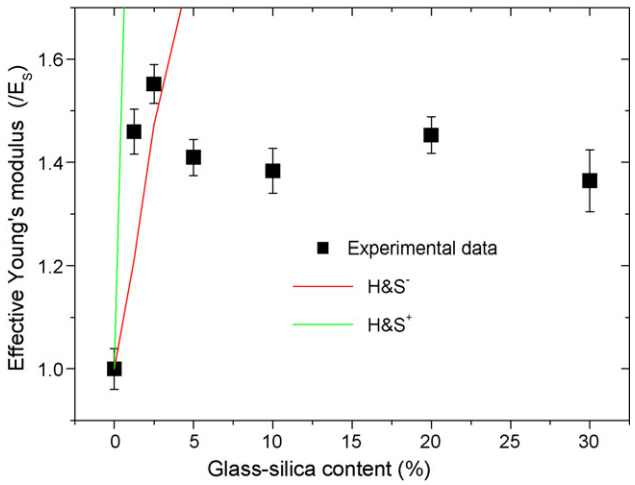

Fig. 10. Observed Young's modulus of starch–glass–silica composite as function of reinforcement content.

Eq. (5) assuming different combinations of t and E_I. In the example shown in Fig. 11a, the effective modulus is plotted against the interphase thickness for different interphase moduli corresponding to the experimental glass fraction $f = 1.25\%$.

The optimal (E_I, t) is obtained when any of the predicted effective moduli equal the experimental value. In this case $E_I = 0.76E_S$ and $t = 5.20\,\mu m$. Note that an equivalent combination (E_I, t) can be obtained for $E_I = 0.38E_S$ if the interphase thickness is further increased. Thus, the same interphase effect can be predicted using either a small interphase thickness combined with a large interphase modulus or vice versa. The interphase thickness represents more than 14% of the particle size. Such ratio is higher than the observed interphase thickness for macroscopic beads.

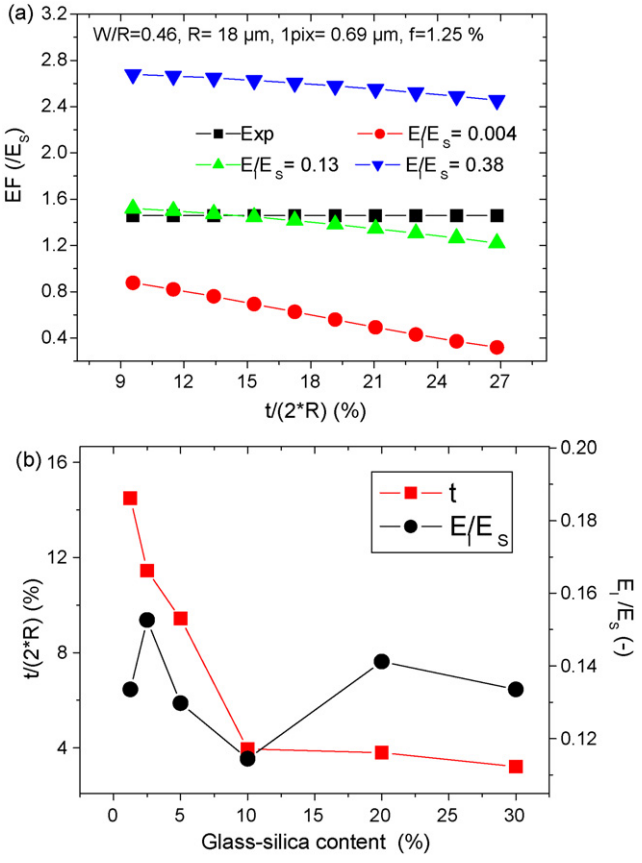

Fig. 11. (a) Identification of the interphase properties based on an inverse strategy. (b) Optimal interphase properties corresponding to the experimental behaviour.

Fig. 11b shows the optimal interphase parameters as function of glass content. The interphase thickness decreases from 5.2 to 1.2 μm, corresponding to interphase thickness/bead size ratio changing from 14 down to 3%. The corresponding interphase modulus is within the range $(0.11–0.15)E_S$. No particular correlation is found between the interphase modulus and the reinforcement content. The interphase modulus is one order of magnitude lower than that of the starch matrix. This result suggests that interphase properties have to be lowered in order to justify the loss of rigidity shown in Fig. 10. Optimal interphase thickness shown in Fig. 11b are in qualitative agreement with the image correlation results (Fig. 6). The average interphase thickness/particle size ratio is about 8% in Fig. 11b, which is the same value observed for macroscopic beads. At this stage, we must admit that interphase properties are scale dependent to explain such matching between experimental and numerical analysis. The origin of such dependent can be attributed to the powder processing where homogeneity of the starch/bead/added water mixture is thought to depend on the filler size. Variability of the interphase properties as function of the filler fraction was observed in the case of an epoxy matrix reinforced by a size mixture of spherical copper particles (Papanicolaou et al., 2008). In that work, the authors showed that their experimental trend is explained by a decrease of matrix–filler adhesion with respect to the filler weight fraction. The degradation of the interphase property does not mean that the composition near the interface is modified. This statement would mean that local melting of glass particles is achieved under low processing temperature, which is not the case. The modification of interphase properties has to deal with varied water content, which, in turn, is dependent on the inter-particle spacing. This hypothesis is confirmed by the image correlation results.

The validity of our model is examined with regards to various analytical and numerical expressions that deal with three-phase models. We compare, first, our results to the model developed by Lutz & Zimmerman (1996). This model gives an exact elastic solution for the case of a functionally graded interphase, i.e., for continuously varied interphase elastic properties between the matrix and the filler. We prove by the way that smoothly graded interphase can be replaced by an effective interphase where the elastic properties are constant through its thickness. The model of Lutz and co-workers predicts the bulk modulus of the effective medium as a function of the interphase properties using the expression:

$$\frac{K_{\text{eff}}}{K_{\text{m}}} = \frac{1 + (4\mu_{\text{m}}/3K_{\text{m}})fc}{1 - fc} \tag{6}$$

where the subscripts eff, m, i, if refer to composite, matrix, particle and interphase, respectively. K and μ are the bulk and shear moduli, respectively. c is the volume fraction of the particles. f is a complex function, which depends on the interphase properties.

$$f = \frac{3(K_{\text{i}} - K_{\text{if}})\sum_{n=0}^{\infty}\Gamma_{n\beta} + (\lambda_{\text{if}} - 2\mu_{\text{if}})\sum_{n=0}^{\infty}n\beta\Gamma_{n\beta}}{3(K_{\text{i}} - K_{\text{if}})\sum_{n=0}^{\infty}\Gamma_{n\beta+3} + (\lambda_{\text{if}} - 2\mu_{\text{if}})\sum_{n=0}^{\infty}(n\beta+3)\Gamma_{n\beta+3}} \tag{7}$$

where λ is Lame's constant.

The following parameters are chosen for the comparison:

$$\begin{aligned} &M_{\text{m}} - \frac{M_{\text{if}}}{M_{\text{m}}} = 0.75 \\ &\nu_{\text{m}} = \nu_{\text{if}} = 0.25 \\ &\beta = 10 \\ &\mu_{\text{i}} = 5\mu_{\text{m}} \end{aligned} \tag{8}$$

where M is the elastic modulus, ν is the Poisson coefficient, β is a parameter that controls the decay of the modulus from the particle.

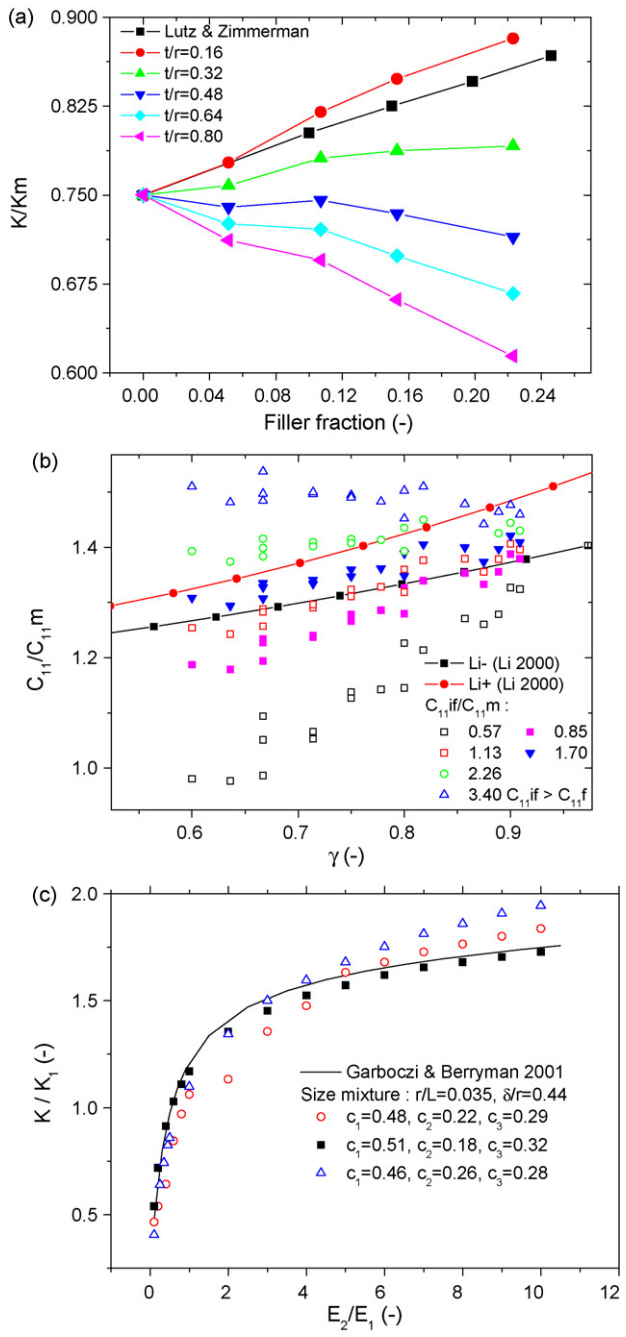

Fig. 12. Comparison between the finite element results with three-phase models from the literature: functionally graded interphase models by (a) Lutz and Zimmerman (1996), (b) Li (2000) and (c) effective medium for uniform interphases by Garboczi and Berryman (2001).

Fig. 12a compares the evolutions of the reduced bulk modulus with respect to the filler fraction. The interphase thickness is scaled with regard to the particle radius. Here, we have used particles of a constant size. We observe that interphase thickness larger than 0.32 decreases the bulk modulus, at least for the filler fractions less than 0.25. The optimal effective interphase thickness, that may represent the functionally graded interphase, seems to be close to 0.20. In the paper of Lutz and Zimmerman (1996), the analysis of the radial stress profile indicates that changes in the stress are limited to a radial distance of about 0.5 times the particle radius.

The second fit deals with the analytical multi-phase model developed by Li (2000). In this model, a linear evolution of the interphase elastic properties is assumed. The model is based on the following effective elastic moduli expression:

$$C_{\text{eff}} = C(I + (S - I)A)(I + SA)^{-1} \tag{9}$$

where all terms refer to tensor quantities defined in Li (2000).

In our comparison, we assume spherical particles of fraction 0.4. Since such a fraction is beyond the percolation threshold, i.e., rigid sphere approximation. We authorise particle overlapping. The elastic moduli contrasts are $E_i/E_m = 2.85$ and $\mu_i/\mu_m = 1.44$. Li uses a scaled interphase parameter i.e., $\gamma = r_i/r_{if}$. We keep in mind that the change of γ imposed in Li (2000) is correlated to the change in the reinforcement fraction keeping constant the matrix volume fraction.

Fig. 12b shows the evolution of Young's modulus as function of the interphase thickness expressed in its reduced form, i.e., $\gamma = r_i/r_{if}$. Also are shown the bounds relative to the functionally graded interphase model. When the matrix is stiffer than the interphase zone, the effective modulus lies below the lower bound. Such a trend is explained by evolving elastic properties of the interphase zone, within the functionally graded model, between those of the filler and the matrix. For an interphase modulus larger than the filler modulus, the effective modulus is beyond the upper bound. The composite modulus is slightly and negatively correlated to γ because of a lower contribution of the stiffest material when γ increases. Finally, we see that good agreement between the present FE model and the functionally graded model (i.e., the predicted FE modulus lies within the bounds) is achievable when the following condition is fulfilled:

$$C_{11m} < C_{11if} < C_{11f} \tag{10}$$

The next comparison refers to the effective medium theory developed in work of Garboczi and Berryman (2001). Their study share common features with the present work because their generated microstructures contain multi-size spherical inclusions within interfacial transition zone exhibiting constant elastic properties. In our work, the size distribution is continuous whereas in Garboczi and Berryman (2001) three sizes are used.

We, again, adjusted the parameters of the present FE model to meet the conditions used in Garboczi and Berryman (2001). For the microstructure containing a matrix fraction of 0.5, the mean size (r/L) and the radii dispersion ($\delta r/r$) are 0.034 and 0.44, respectively. L refers to the size of the digital image, which is adjusted to 1000 as in Garboczi and Berryman (2001). With such a resolution, one FE run takes 5 min on a Quad core computer. The average interphase thickness (t/r) is 0.37. Young's moduli contrast between the stiff filler and the compliant matrix is $E_1/E_2 = 0.2$. Note that, for seek of clarity, we use the same lettering as in Garboczi and Berryman (2001). The interphase thickness is adjusted in a way to keep the surface fraction of the interphase, matrix and filler similar to those values in the above-mentioned work.

Fig. 12c compares the FE and the differential effective medium theory results expressed as composite modus vs. normalised interphase modulus. All trends well show that the composite bulk modulus rapidly increases before attaining a steady-state stage when the interphase modulus increases. The steep regime is correlated to the replacement of the matrix phase by a stiffer material, i.e., the interphase. Further increase of the interphase modulus does not affect the trend because the interphase fraction does not change.

Changes in the size–mixture parameters (r/L, σ/r) also do not affect the result as long as the phase fractions c_1, c_2 and c_3 are kept at the same levels (results not shown). Note that "result" means effective property and not the stress distribution. In the counter part, any variation in the interphase fraction c_2 has the consequence to increase further the effective modulus at a given E_2/E_1 ratio (Fig. 12c).

5. Conclusions

The effective Young's modulus of starch-based composites reinforced using glass particles is increased up to a limiting fraction of 1.25 wt.%. Further increase of the reinforcement content leads to an asymptotic modulus of about $1.4E_S$, where E_S is the starch modulus. Finite element results show that the three-phase model is able to capture the experimental behaviour. The predicted Young's modulus is nicely correlated to the interphase content in the microstructure. Interphase content should be considered as the main variable in the effective law instead of the filler fraction, especially when imperfect interface action is correlated to a significant alteration of the matrix–filler load transfer. In order to fit the observed modulus with respect to glass fraction, the interphase modulus is predicted ten times lower than that of the starch matrix. The predicted interphase thickness represents few percents of the bead size.

The comparison between the present FE model and analytical models shows, first, that functionally graded the interphase can be replaced by constant interphase properties giving particular windowing of the interphase properties. This statement is not a rigid truth, in the sense that the stress distributions are not equivalent for the two models. The study of particular deformation mechanisms such as in damage or fracture growth certainly give different results. The FE model also compares very well with the effective medium theory for interphases exhibiting constant properties across their thickness. The control of the filler size mixture in a way to adjust the interphase fraction has the leading role on the modification of the effective modulus.

Acknowledgements

The authors would like to thank D. Lourdin and L. Chaunier from BIA for their technical assistance.

References

Agbossou, A. (1995). The effect of interphase and impact strain rates on tensile off-axis behaviour of unidirectional glass fibre composite: Experimental results. *Engineering Fracture Mechanics*, *52*(5), 923–934.

Alem, N., & Dravid, V. P. (2008). Correlative deformation mechanisms in $Ni_xCo_{1-x}O/ZrO_2(CaO)$ directionally solidified eutectic composites with a confined metallic interphase. *Acta Materialia*, *56*, 4378–4389.

Alfano, G., & Criseld, M. A. (2001). Finite element interface models for the delamination analysis of laminated composites: Mechanical and computational issues. *International Journal for Numerical Methods in Engineering*, *50*, 1701–1736.

Ash, J. T., Cross, W. M., Svalstad, D., Kellar, J. J., & Kjerengtroen, L. (2003). Finite element evaluation of the microbond test: Meniscus effect, interphase region, and vise angle. *Composites Science and Technology*, *63*, 641–651.

Beg, M. D. H., Pickering, K. L., & Weal, S. J. (2005). Corn gluten meal as a biodegradable matrix material in wood fibre reinforced composites. *Materials Science and Engineering A*, *412*(1–2), 7–11.

Benveniste, Y. (2006). A general interface model for a three-dimensional curved thin anisotropic interphase between two anisotropic media. *Journal of the Mechanics and Physics of Solids*, *54*, 708–734.

Benveniste, Y., & Miloh, T. (2001). Imperfect soft and stiff interfaces in two-dimensional elasticity. *Mechanics of Materials*, *33*(6), 309–323.

Biliaderis, C. G., Lazaridou, A., & Arvanitoyannis, I. (1999). Glass transition and physical properties of polyol-plasticised pullulan–starch blends at low moisture. *Carbohydrate Polymers*, *40*(1), 29–47.

Chaboche, J. L., Girard, R., & Schaff, A. (1997). Numerical analysis of composite systems by using interphase/interface models. *Computational Mechanics*, *20*, 3–11.

Chandra, N., & Ananth, C. R. (1995). Analysis of interfacial behavior in MMCs and IMCs by the use of thin-slice push-out tests. *Composites Science and Technology*, *54*, 87–100.

Chandra, N., & Ghonem, H. (2001). Interfacial mechanics of push-out tests: Theory and experiments. *Composites Part A: Applied Science and Manufacturing*, *32*, 575–584.

Chaudhry, T. M., Ho, H., Drzal, L. T., Harris, M., & Laine, R. M. (1995). Silicon oxycarbide coatings on graphite fibers II. Adhesion, processing, and interfacial properties. *Materials Science and Engineering A*, *195*, 237–249.

Cheeseman, B. A., & Santare, M. H. (2001). The effect of the interphase on crack–inclusion interactions. *International Journal of Fracture*, *109*, 303–323.

Chicot, D., Démarécaux, P., & Lesage, J. (1996). Apparent interface toughness of substrate and coating couples from indentation tests. *Thin Solid Films*, *283*(1–2), 151–157.

Choi, I. S., Detor, A. J., Schwaiger, R., Dao, M., Schuh, C. A., & Suresh, S. (2008). Mechanics of indentation of plastically graded materials – II: Experiments on nanocrystalline alloys with grain size gradients. *Journal of the Mechanics and Physics of Solids*, *56*(1), 172–183.

Chu, Y. C., & Rokhlin, S. I. (1995). Determination of fiber–matrix interphase moduli from experimental moduli of composites with multi-layered fibers. *Mechanics of Materials*, *21*, 191–215.

Dehm, G., Ruhle, M., Conway, H., & Raj, R. (1997). A microindentation method for estimating interfacial shear strength and its use in studying the influence of titanium transition layers on the interface strength of epitaxial copper films on sapphire. *Acta Materialia*, *45*(2), 489–499.

Duan, H. L., Wang, J., Huang, Z. P., & Karihaloo, B. L. (2005). Size-dependent effective elastic constants of solids containing nano-inhomogeneities with interface stress. *Journal of the Mechanics and Physics of Solids*, *53*(7), 1574–1596.

Esmaeili, N., & Tomita, Y. (2006). Micro- to macroscopic responses of a glass particle-blended polymer in the presence of an interphase layer. *International Journal of Mechanical Sciences*, *48*, 1186–1195.

Gao, S. L., & Mader, E. (2002). Characterisation of interphase nano-scale property variations in glass fibre reinforced polypropylene and epoxy resin composites. *Composites Part A: Applied Science and Manufacturing*, *33*(4), 559–576.

Garboczi, E. J., & Bentz, D. P. (1997). Analytical Formulas for interfacial transition zone properties. *Advanced Cement Based Materials*, *6*(3–4), 99–108.

Garboczi, E. J., & Berryman, J. G. (2001). Elastic moduli of a material containing composite inclusions: Effective medium theory and finite element computations. *Mechanics of Materials*, *33*, 455–470.

Gáspár, M., Benkő, Z., Dogossy, G., Réczey, K., & Czigány, T. (2005). Reducing water absorption in compostable starch-based plastics. *Polymer Degradation and Stability*, *90*(3), 563–569.

Giancaspro, J., Papakonstantinou, C., & Balaguru, P. (2008). Fire resistance of inorganic sawdust biocomposite. *Composites Science and Technology*, *68*(7–8), 1895–1902.

Gross, R. A., & Kalra, B. (2002). Biodegradable polymers for the environment. *Science*, *298*, 803–807.

Guessasma, S., & Benseddiq, N. (2009). Cohesive bonding interface model for the effective properties of randomly structured composites. *Computational Materials Science*, *47*(1), 186–192.

Guessasma, S., Sehaki, M., Lourdin, D., & Bourmaud, A. (2008). Viscoelasticity properties of biopolymer composite materials determined using finite element calculation and nanoindentation. *Computational Materials Science*, *44*(2), 371–377.

Hashin, Z. (2002). Thin interphase/imperfect interface in elasticity with application to coated fiber composites. *Journal of the Mechanics and Physics of Solids*, *50*(12), 2509–2537.

Hashin, Z., & Monteiro, P. J. M. (2002). An inverse method to determine the elastic properties of the interphase between the aggregate and the cement paste. *Cement and Concrete Research*, *32*(8), 1291–1300.

Ho, H., & Dual, L. T. (1996). Evaluation of interfacial mechanical properties of fiber reinforced composites using the microindentation method. *Composites Part A: Applied Science and Manufacturing*, *27A*, 961–971.

Hodzic, A., Stachurski, Z. H., & Kim, J. K. (2000). Nano-indentation of polymer–glass interfaces Part I. Experimental and mechanical analysis. *Polymer*, *41*(18), 6895–6905.

Igawa, N., Taguchi, T., Yamada, R., Ishii, Y., & Jitsukawa, S. (2007). Mechanical properties of SiC/SiC composite with magnesium–silicon oxide interphase. *Journal of Nuclear Materials*, *367–370*, 725–729.

Johnson, A. C., Hayes, S. A., & Jones, F. R. (2009). Data reduction methodologies for single fibre fragmentation test: Role of the interface and interphase. *Composites Part A*, *40*, 449–454.

Kari, S., Berger, H., Gabbert, U., Guinovart-Dıaz, R., Bravo-Castillero, J., & Rodrıguez-Ramos, R. (2008). Evaluation of influence of interphase material parameters on effective material properties of three phase composites. *Composites Science and Technology*, *68*, 684–691.

Kharrat, M., Chateauminois, A., Carpentier, L., & Kapsa, P. (1997). On the interfacial behaviour of a glass/epoxy composite during a micro-indentation test: Assessment of interfacial shear strength using reduced indentation curves. *Composites Part A: Applied Science and Manufacturing*, *28A*, 39–46.

Kim, S. (2008). Processing and properties of gluten/zein composite. *Bioresource Technology*, *99*(6), 2032–2036.

Kunanopparat, T., Menut, P., Morel, M.-H., & Guilbert, S. (2008). Reinforcement of plasticized wheat gluten with natural fibers: From mechanical improvement to deplasticizing effect. *Composites Part A*, *39*, 777–785.

Lamon, J. (2001). A micromechanics-based approach to the mechanical behavior of brittle–matrix composites. *Composites Science and Technology*, *61*(15), 2259–2272.

Lee, S., Wang, S., Pharr, G., & Xu, H. (2007). Evaluation of interphase properties in a cellulose fiber-reinforced polypropylene composite by nanoindentation and finite element analysis. *Composites Part A: Applied Science and Manufacturing*, *38*, 1517–1524.

Li, J. Y. (2000). Thermoelastic behavior of composites with functionally graded interphase: A multi-inclusion model. *International Journal of Solids and Structures*, *37*, 5579–5597.

Li, S., Dickinson, L. C., & Chinachoti, P. (1998). Mobility of "unfreezable" and "freezable" water in waxy corn starch by 2H and 1H NMR. *Journal of Agricultural and Food Chemistry*, *46*, 62–71.

Li, W., & Siegmund, T. (2004). An analysis of the indentation test to determine the interface toughness in a weakly bonded thin film coating–substrate system. *Acta Materialia*, *52*, 2989–2999.

Lipkin, D. M., Clarke, D. R., & Evans, A. G. (1998). Effect of Interfacial carbon on adhesion and toughness of gold-sapphire interfaces. *Acta Materialia*, *46*(13), 4835–4850.

Lissenden, C. J., & Herakovich, C. T. (1995). Numerical modelling of damage development and viscoplasticity in metal matrix composites. *Computer Methods in Applied Mechanics and Engineering*, *126*, 289–303.

Liu, L., Song, Y. J., Fu, H. J., Jiang, Z. X., Zhang, X. Z., Wu, L. N., et al. (2008). The effect of interphase modification on carbon fiber/polyarylacetylene resin composites. *Applied Surface Science*, *254*, 5342–5347.

Lutz, M. P., Menteiro, P. J. M., & Zimmerman, R. W. (1997). Inhomogeneous interfacial transition zone model for the bulk modulus of mortar. *Cement and Concrete Research*, *27*(7), 1113–1122.

Lutz, M. P., & Zimmerman, R. W. (1996). Effect of the interphase zone on the bulk modulus of a particulate composite. *Journal of Applied Mechanics*, *63*, 855–861.

Lutz, M. P., & Zimmerman, R. W. (2005). Effect of an inhomogeneous interphase zone on the bulk modulus and conductivity of a particulate composite. *International Journal of Solids and Structures*, *42*, 429–437.

Ma, L., & Wen, J. (2008). Biocomposite of double-walled carbon nanotube-doped alginate gel for biomaterial immobilization. *Composites Science and Technology*, *68*, 1297–1303.

Mann, K. A., Miller, M. A., Race, A., & Verdonschot, N. (2009). Shear fatigue micromechanics of the cement–bone interface: An in vitro study using digital image correlation techniques. *Journal of Orthopaedic Research*, *27*(3), 340–346.

Munz, M., Sturm, H., Schulz, E., & Hinrichsen, G. (1998). The scanning force microscope as a tool for the detection of local mechanical properties within the interphase of fibre reinforced polymers. *Composites Part A*, *29A*, 1251–1259.

Naslain, R., Lamon, J., Pailler, R., Bourrat, X., Guette, A., & Langlais, F. (1999). Micro/minicomposites: A useful approach to the design and development of non-oxide CMCs. *Composites Part A: Applied Science and Manufacturing*, *30*, 537–547.

Nozawa, T., Katoh, Y., & Snead, L. L. (2009). The effect of neutron irradiation on the fiber/matrix interphase of silicon carbide composites. *Journal of Nuclear Materials*, *384*, 195–211.

Papanicolaou, G. C., Xepapadaki, A. G., Kotrotsos, A., & Mouzakis, D. E. (2008). Interphase modeling of copper–epoxy particulate composites subjected to static and dynamic loading. *Journal of Applied Polymer Science*, *109*, 1150–1160.

Patel, R. K., Bhattacharya, B., & Basu, S. (2008). Effect of interphase properties on the damping response of polymer nano-composites. *Mechanics Research Communications*, *35*, 115–125.

Pompidou, S., & Lamon, J. (2007). Analysis of crack deviation in ceramic matrix composites and multilayers based on the Cook and Gordon mechanism. *Composites Science and Technology*, *67*, 2052–2060.

Rjafiallah, S., Guessasma, S., Chaunier, L., & Lourdin, D. (2009). Effective properties of starch-based composites subject to interface effect. In *7th EUROMECH solid mechanics conference* Lisbon, Portugal.

Rjafiallah, S., Guessasma, S., & Lourdin, D. (2009). Effective properties of biopolymer composites: A three phase finite element model. *Composites A*, *40*(2), 130–136.

Rokhlin, S. I., & Huang, W. (1998). Micromechanical analysis and ultrasonic characterization of interphases and interphasial damage in high temperature composites. *Composites Part B: Engineering*, *29B*, 147–157.

Rokhlin, S. I., Huang, W., & Chu, Y. C. (1995). Ultrasonic scattering and velocity methods for characterization of fibre–matrix interphases. *Ultrasonics*, *33*(5), 351–364.

Ru, C. Q. (1999). A new method for an inhomogeneity with stepwise graded interphase under thermomechanical loadings. *Journal of Elasticity*, *56*, 107–127.

Ruan, R., Almaer, S., Huang, V., Perkins, P., Chen, P., & Fulcher, R. G. (1996). Relationship between firming and water mobility in starch-based food systems during storage. *Cereal Chemistry*, *73*(3), 328–332.

Scheffler, C., Gao, S. L., Plonka, R., Mäder, E., Hempel, S., Butler, M., et al. (2009). Interphase modification of alkali-resistant glass fibres and carbon fibres for textile reinforced concrete I: Fibre properties and durability. *Composites Science and Technology*, *69*, 531–538.

Segurado, J., & LLorca, J. (2004). A new three-dimensional interface finite element to simulate fracture in composites. *International Journal of Solids and Structures*, *41*, 2977–2993.

Sevostianov, I., & Kachanov, M. (2007). Effect of interphase layers on the overall elastic and conductive properties of matrix composites. Applications to nanosize inclusion. *International Journal of Solids and Structures*, *44*(3–4), 1304–1315.

Shen, H., Schiavone, P., & Potapenko, S. (2005). Thermal behavior of an elliptic inhomogeneity surrounded by a compliant interphase layer. *Mechanics of Materials*, *37*, 663–675.

Shen, L., & Li, J. (2005). Homogenization of a fibre/sphere with an inhomogeneous interphase for the effective elastic moduli of composites. *Proceedings of the Royal Society A: Mathematical Physical and Engineering Sciences*, *461*(2057), 1475–1504.

Sun, Z., Garboczi, E. J., & Shah, S. P. (2007). Modeling the elastic properties of concrete composites: Experiment, differential effective medium theory, and numerical simulation. *Cement and Concrete Composites*, *29*, 22–38.

Taliercio, A. (2007). Macroscopic strength estimates for metal matrix composites embedding a ductile interphase. *International Journal of Solids and Structures*, *2007*, 7213–7238.

Tasdemir, M., Tasdemir, C., Akyuz, S., Jefferson, A., Lydon, F., & Barr, B. (1998). Evaluation of strains at peak stresses in concrete: A three-phase composite model approach. *Cement and Concrete Composites*, *20*(4), 301–318.

Tharanathan, R. N. (2003). Biodegradable films and composite coatings: Past, present and future. *Trends in Food Science and Technology*, *14*(3), 71–78.

Tillman, M., Hayes, B., & Seferis, J. (2000). Analysis of polymeric composite interphase regions with thermal atomic force microscopy. *Journal of Applied Polymer Science*, *80*(10), 1643–1649.

Tripathi, D., & Jones, F. R. (1997). Measurement of the load-bearing capability of the fibre/matrix interface by single-fibre fragmentation. *Composites Science and Technology*, *57*, 925–935.

Tsui, C., Tang, C., & Lee, T. (2001). Finite element analysis of polymer composites filled by interphase coated particles. *Journal of Materials Processing Technology*, *117*(1–2), 105–110.

Tvergaard, V. (2009). Analyses of crack growth in ductile metals. In J. Ambrosio, & M. P. T. Silva (Eds.), *7th Euromech solid mechanics conference (p. 499)*. Lisbon, Portugal: APMTAC.

Urena, A., Rams, J., Escalera, M. D., & Sanchez, M. (2005). Characterization of interfacial mechanical properties in carbon fiber/aluminium matrix composites by the nanoindentation technique. *Composites Science and Technology*, *65*(13), 2025–2038.

Wang, J., Duan, H., Zhang, Z., & Huang, Z. P. (2005). An anti-interpenetration model and connections between interphase and interface models in particle-reinforced composites. *International Journal of Mechanical Sciences*, *47*, 701–718.

Wang, X. D., & Meguid, S. A. (1999). Dynamic interaction between a matrix crack and a circular inhomogeneity with a distinct interphase. *International Journal of Solids and Structures*, *36*, 517–531.

Wang, X., & Zhong, Z. (2003). A circular inclusion with a nonuniform interphase layer in anti-plane shear. *International Journal of Solids and Structures*, *40*, 881–897.

Wei, P. J., & Huang, Z. P. (2004). Dynamic effective properties of the particle-reinforced composites with the viscoelastic interphase. *International Journal of Solids and Structures*, *41*, 6993–7007.

Weissmuller, J., & Cahn, J. (1997). Mean stresses in microstructures due to interface stresses: A generalization of a capillary equation for solids. *Acta Materialia*, *45*(5), 1899–1906.

Wu, Q. X., Sakabe, H., & Isobe, S. (2003). Processing and properties of low cost corn gluten meal/wood fiber composite. *Industrial and Engineering Chemistry Research*, *42*(26), 6765–6773.

Zhang, H., Chen, Q., & Li, D. (2004). Development of a novel lateral force-sensing microindentation technique for determination of interfacial bond strength. *Acta Materialia*, *52*(7), 2037–2046.

Zhang, W. X., Li, L. X., & Wang, T. J. (2007). Interphase effect on the strengthening behavior of particle-reinforced metal matrix composites. *Computational Materials Science*, *41*, 145–155.

Zhou, X., Wagner, H., & Nutt, S. (2001). Interfacial properties of polymer composites measured by push-out and fragmentation tests. *Composites Part A: Applied Science and Manufacturing*, *32*(11), 1543–1551.

Zhu, W., & Bartos, P. (1997). Assessment of interfacial microstructure and bond properties in aged GRC using a novel microindentation method. *Cements and Concrete Composites*, *27*(11), 1701–1711.